# NONDESTRUCTIVE RULE-BASED DEFECT DETECTION AND IDENTIFICATION SYSTEM IN CT IMAGES OF HARDWOOD LOGS

Erol Sarigul[1], A. Lynn Abbott[1], and Daniel L. Schmoldt[2]

[1] *Bradley Department of Electrical and Computer Engineering, Virginia Tech, Blacksburg, Virginia 24061, USA*

[2] *USDA Forest Service, Biological Systems Engineering Dept., 460 Henry Mall, University of Wisconsin, Madison, Wisconsin 53706, USA*

**Abstract.** This paper is concerned with the detection of internal defects in hardwood logs. Because the commercial value of hardwood lumber is directly related to the quantity, type, and location of defects in the wood, sawing strategies are typically chosen in an attempt to minimize the defects in the resulting boards. Traditionally, the sawyer makes sawing decisions by visually examining the exterior of log and then revising the sawing strategy as more and more of the log's interior is exposed. Significantly better results would be expected if internal defects were known, so that a globally optimum solution could be selected in advance. This paper addresses this problem through the analysis of computed tomography (CT) images of logs, for the purpose of detecting important hardwood defects. In particular, the paper considers defect-dependent postprocessing methods, based on mathematical morphology, that show promising results.

## INTRODUCTION

Increasing prices and limited forest resources continue to drive the hardwood industry to seek more productive means of converting logs to lumber. Conventional log sawing practices waste considerable amounts of valuable wood, largely because most defects that adversely affect board quality are at unknown locations inside the logs. Studies have shown, for example, that the commercial value of lumber can be improved by 11% to 21% through the careful selection of sawing strategies, particularly if internal defect locations were known [1-3].

Previous studies have demonstrated the ability to detect important internal defects through the analysis of computed tomography (CT) images of logs. For example, some early studies are presented in [4-6]. Zhu et al. [7] described a segmentation approach that relied heavily on edge and texture measures. Bhandarkar et al. [8] described an correlation-based approach to defect detection. Schmoldt et al. [9-11] described an approach that used artificial neural nets (ANN) to classify pixels individually, using small neighborhoods of CT density values as input feature vectors.

In general, the problem is difficult because of the inherently variability of wood. Although much of the work reported above has yielded results that are good in a quantitative sense, subjective evaluation suggests that the results could be improved in a qualitative sense by refining the resulting shapes and extent of detected defect regions in the images. For example, small spurious defect regions may have only a small effect on pixel-wise statistical classification accuracy, but are objectionable to the human observer. In

CP557, *Review of Progress in Quantitative Nondestructive Evaluation Vol. 20,* ed. by D. O. Thompson and D. E. Chimenti

many cases, such regions can be identified and eliminated easily. The goal of this paper is to describe recent attempts accomplish this. (See also the related work that is described in [12].)

Initial classification is performed using local neighborhoods of CT density values. These serve as input values to an ANN, which assigns a label ("knot," "decay," "split", "bark," or "clear wood") to each pixel in the image. The postprocessing module that is described here uses higher-level, domain-dependent knowledge to refine initial classification results. There are several motivations for such an approach. First, the initial ANN-based classifier depends primarily on information from very small image neighborhoods, and identifies defects on a pixel-by-pixel basis. It therefore ignores such information such as defect shape, size, and position within the log. Second, the rule-based postprocessing approach that we describe here can employ fundamentally different types of rules for different defects, whereas the ANN approach that we use is restricted to a single topology for all classes that it can identify.

The next section of this paper presents a system overview. Because the postprocessing system depends heavily on mathematical morphology, some fundamental definitions of mathematical morphology are given in the section that follows. The next two sections provide example postprocessing results for two defect types, bark and splits. The merging of separate postprocessing results is then discussed, and the last section presents concluding remarks.

## SYSTEM OVERVIEW

The overall classification system consists of three modules: (1) a preprocessing module, (2) an artificial neural network (ANN) module that assigns tentative labels, and (3) a postprocessing module which is the primary topic of this paper. The preprocessing module distinguishes wood from background (air) and internal voids, and normalizes CT density values. The ANN module labels each non-background pixel of a CT slice using histogram-normalized values from small windows of size 3×3×3 or 5×5, centered on pixel location to be classified. In the postprocessing module, morphological operations are preformed to remove spurious regions and refine region shapes. Individual region types are considered individually, and are then merged to form a single segmented image.

## MATHEMATICAL MORPHOLOGY BASICS

Mathematical morphology, also known as image algebra, is the study of shape or form using the tools of set theory [13-15]. Mathematical morphology operations can be used to modify image shapes, reduce noise, and detect features of interest.

In this paper, we consider only binary images and binary morphology. In this case, only two different pixel values are possible, often called "foreground" and "background" levels. It is possible to represent a binary image as a set of (row, column) coordinate locations for all of the foreground points. Most morphology operations involve a *structuring element*, which is another set of (row, column) pairs. The structuring element is typically quite small, and its shape has a direct impact on the results.

In the following discussion, it will be convenient to use subscript notation to represent the *translation* of a set:

$$(A)_x = \{a + x \mid a \in A\}. \tag{1}$$

Two fundamental operations of mathematical morphology are *dilation* and *erosion*. Intuitively, these operations tend to enlarge and reduce (respectively) the sizes of foreground regions in images. Let set $A$ represent a binary image, and let $B$ represent a structuring element. A definition of dilation is

$$A \oplus B = \{a + b \mid a \in A \text{ and } b \in B\} \tag{2}$$

and a definition of erosion is

$$A \ominus B = \{x \mid (B)_x \subseteq A\} \tag{3}$$

The successive application of these two operations is common. The morphological *opening* of $A$ by $B$ is defined as

$$A \circ B = (A \ominus B) \oplus B \tag{4}$$

and *closing* is given by

$$A \bullet B = (A \oplus B) \ominus B \tag{5}$$

A few other terms will also be needed later in the paper. The *complement* of a set can be written as

$$A^C = \{x \mid x \notin A\} \tag{6}$$

The *Minkowski difference* of two sets $A$ and $B$ is defined as

$$A \setminus B = \{x \mid x \in A \text{ and } x \notin B\} = A \cap B^C \tag{7}$$

## REFINEMENT OF BARK REGIONS

In order to show how domain-dependent rules can be developed and applied, we begin with an example concerning bark. Because the density of bark is very close to that of clear wood, the ANN can confuse the two types relatively easily. In this application, it is reasonably to assume that bark should lie on the outside of a log. (We ignore the case of included bark for the present.) It is therefore possible to state this simple rule: Retain only those bark regions in the image that lie at the outer boundary of the log. The high-level processing strategy is first to determine which points lie on the outside edge of the log, and then to retain only those bark regions that overlap one or more boundary points.

Let us first consider morphological postprocessing operations that can be used to obtain the boundary, as shown in Fig. 1. Fig. 1(a) shows an image of a red oak log that has lost most of its bark, except for the upper right and lower left portions of the image. A binary log image, in which dark foreground points represent the log, is shown in Figure 1(b). This binary image is dilated using a 3 × 3 structuring element, and points associated with Fig. 1(b) are removed from the dilated version. The result is a representation of the log's boundary, as shown in Fig. 1(c), and will be used in subsequent processing. Algebraically, the procedure can be written as

$$C = (A \oplus B) \setminus A \tag{8}$$

where $A$ is the binary log image, $B$ is the structuring element, and $C$ is the result. Notice that the structuring element can be expressed formally as $B$ = {(-1, -1), (-1, 0), (-1, 1), (0, -1), (0, 0), (0, 1),(1, -1), (1, 0), (1, 1)}. Dilation by this structuring element causes $A$ to be enlarged by one pixel in every direction.

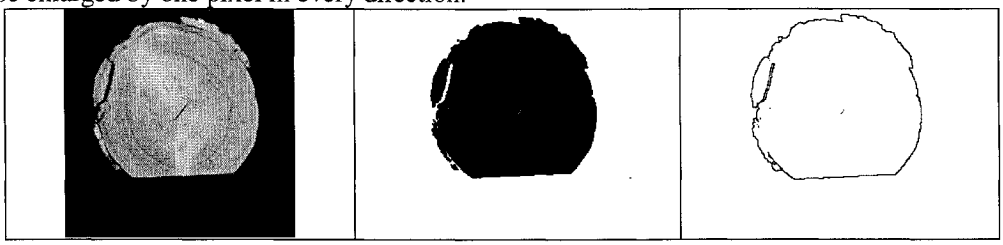

(a) (b) (c)

**Figure 1.** Postprocessing example for bark. (a) CT image slice of red oak log. (b) Foreground points associated with the log. (c) The detected outside boundary of the log.

The next step is to eliminate bark regions detected by the ANN that do not touch the boundary. Initial bark regions for this image, as labeled by the ANN, are shown in Fig. 2(a). In this example, several small regions have been incorrectly labeled as bark, and a fairly large region near the top has also been incorrectly labeled. We first apply morphological opening to the initial bark region, using the same structuring element that is used in the extraction of the log's boundary. This removes small "necks" that connect larger regions, smoothes region boundaries, and additionally removes some of the smaller regions from further consideration. The result is shown in Fig. 2(b). To this image we apply *conditional dilation*. This is an iterative procedure that retains only those regions that are designated initially using *marker points*. In our case all foreground points in the boundary image $C$ (Fig. 1(c)) are employed as marker points. $C$ is repeatedly dilated using the 3×3 structuring element $B$, but at every iteration the intermediate result is intersected with the bark image given in Fig. 2(b). We designate this input bark image as $I_{bark}$, and it serves formally as a "mask" image for the conditional dilation. The conditional dilation can be expressed as

$$I_{bark\_new} = (C \oplus B)^{(i)} \cap I_{bark} \tag{9}$$

where the superscript $(i)$ represents the repetition index. The dilations and intersections continue until no change occurs; i.e., $(C \oplus B)^{(i)} \cap I_{bark} = (C \oplus B)^{(i+1)} \cap I_{bark}$. The result of this is shown in Fig. 2(c). The postprocessing steps for bark are summarized in the diagram of Fig. 3.

(a) (b) (c)

**Figure 2.** Continued processing for bark. (a) Bark image. The dark points represent bark, as tentatively identified by the ANN. (b) The result of morphological opening. (c) The result after removing regions not on the boundary of the log.

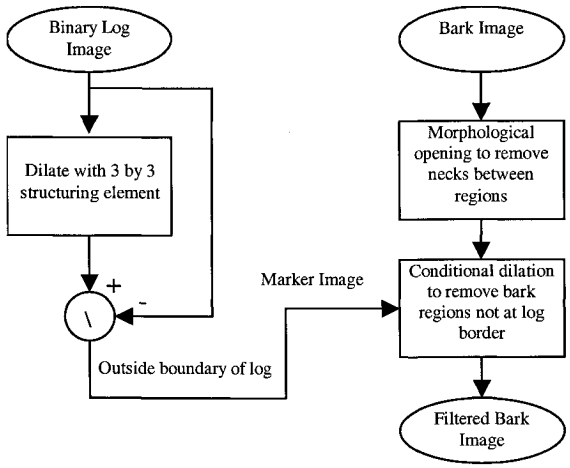


**Figure 3.** Postprocessing of bark regions. Relatively simple morphological processing leads to significantly improved results for the example shown.

## REFINEMENT OF SPLIT REGIONS

A split is a longitudinal and radial separation of the wood, due to the tearing apart of wood cells. Postprocessing operations can be selected to take advantage of the narrow, elongated shapes that are expected of split regions.

The flowchart procedure for this is given in Fig. 4. First, a majority filter is applied to partially eliminate problems due to annual rings. The majority algorithm considers the 9 pixels within each 3×3 neighborhood. Because pixels can have only foreground or background values, more than half of the 9 pixels must have one of these two values. That value replaces the value at the center pixel. Next, morphology operations are employed to extract a *skeleton* of each region. A skeleton is a thinned representation of a region that retains information associated with its original size, orientation, and connectivity. Lantuéjoul showed that the skeleton of a binary image $A$ could be expressed in terms of morphological erosions and openings [16]. With $S(A)$ denoting the skeleton of $A$, it can be shown that

$$S(A) = \bigcup_{k=0}^{K} S_k(A) \tag{10}$$

with

$$S_k(A) = \bigcup_{k=0}^{K} \left\{ (A \ominus kB) \setminus \left[ (A \ominus kB) \circ B \right] \right\} \tag{11}$$

where $B$ is a structuring element, $(A \ominus kB)$ indicates $k$ successive erosions of $A$, and $K$ is the number of steps before $A$ erodes to an empty set:

$$K = \max \left\{ k \mid (A \ominus kB) \neq \varnothing \right\} . \tag{12}$$

The skeletonization procedure will typically produce a thinned image in which some small, spurious regions remain. We now remove these, eliminating all regions having an area that is smaller than an empirically chosen threshold.

Because splits are very narrow, they are often difficult to detect in CT images. Because of this, splits are often detected by the ANN as separate regions that need to be linked. For the case that 2 or more split regions are present, we now apply a linking step that searches for skeleton endpoints that lie in close proximity. If the distance is sufficiently small between any two endpoints from different skeletons, then these two endpoints are joined by a straight line.

It is relatively simple to find the endpoints of skeletons, using morphological *hit-or-miss* operations [17] with the different templates depicted in Fig. 5. Each template represents a particular type of endpoint configuration to be matched in the image.

After linking nearby skeletons, we refine the resulting regions by applying a morphological *pruning* algorithm to remove small, spurious branches. Conceptually, this is accomplished by repeatedly detecting skeleton endpoints and removing those endpoints. However, if this is performed directly, the main branches of the skeletons will be shortened as the small spurs are removed. To avoid this problem, we have adopted a skeleton filtering procedure introduced by Soille [17]. With this technique, spurious branches are removed without shortening the main branches that represent splits.


**Figure 4.** Postprocessing procedure for split regions. Because splits are often very narrow, they can be difficult to detect in CT images.

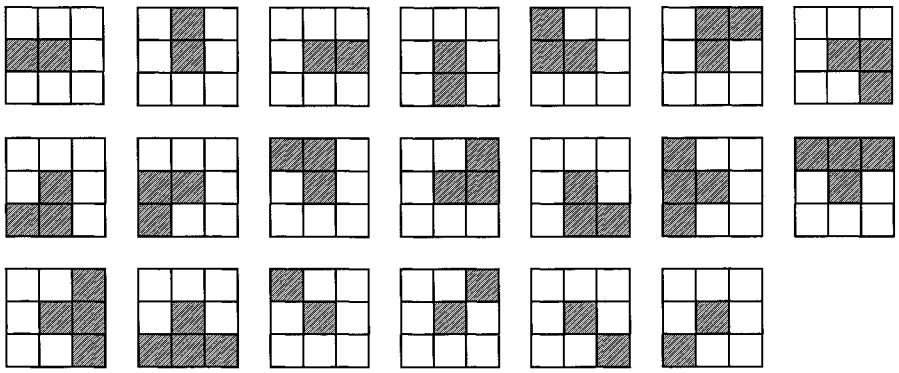

**Figure 5.** Structuring elements for endpoint detection. Each grid of 9 points represents a pair of structuring elements. In each case, the dark cells represent the set of foreground pixels, and the white cells represent the set of background pixels.

A typical example of split postprocessing is shown in Fig. 6. The CT image in Fig. 6a is used for ANN classification. The output of the ANN classifier is shown in Fig. 6b. The majority-filtering algorithm eliminates most annual rings (Fig. 6c), and skeletonization thins all of the resulting regions to 1-pixel widths (Fig. 6d). Small regions are then removed (Fig. 6e), and the remaining connected components are linked (Fig. 6f). Finally, most spurious branches are removed from the resulting split region, while keeping the main branch unchanged (Fig. 6g). In this case, the result is not perfect; a connected side split (barely visible at the 2 o'clock position in the image) is eventually eliminated by these steps. It is a sub-pixel resolution split that is difficult even for the human eye to detect.

## MERGING THE RESULTS

After postprocessing the individual layers separately (knots, splits, bark, and decay, and clear wood), we need to combine all separated layers into a final image.

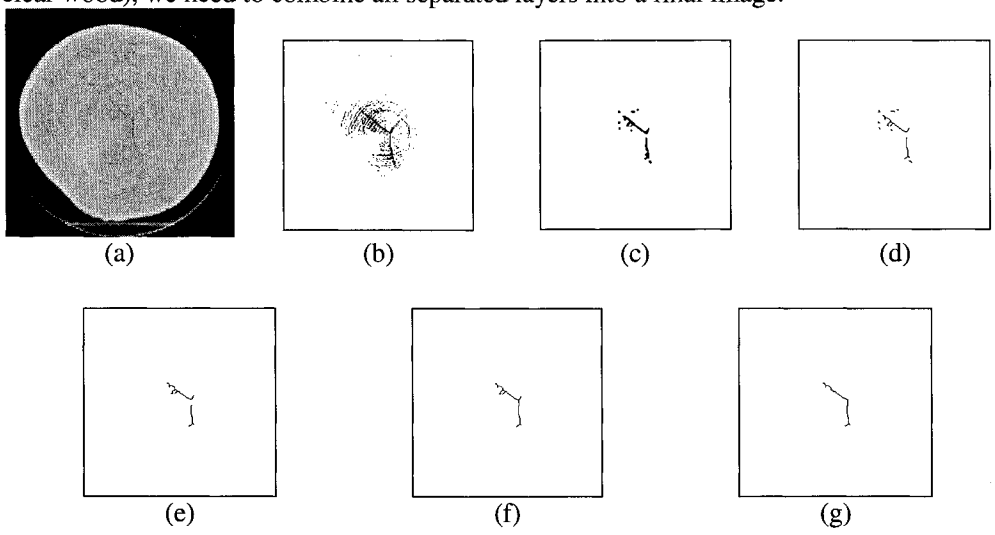


**Figure 6.** Postprocessing of split regions. (a) Example of red oak image with prominent split. (b) Split pixels, as tentatively assigned by the ANN. (c) The result of majority filtering algorithm. (d) Result of skeletonization. (e) Result of spurious object removal. (f) Result of branch linking. (g) Result of final skeleton filtering.

**Table 1.** Precedence rules to resolve pairs of overlapping labels. The unshaded labels in the table represent the "winners" for cases that two labels (one shaded label from the left, and one shaded label from the bottom) have been assigned to a single pixel.

| | | | | |
|---|---|---|---|---|
| Knot | Knot | | | |
| Split | Split | Split | | |
| Decay | Decay | Knot | Split | |
| Bark | Bark | Bark | Bark | Bark |
| | Clear Wood | Knot | Split | Decay |

(Because of page limitations, we do not discuss the postprocessing of other defects here.) However, some defect regions will have grown, causing some regions from different layers to overlap. To resolve those overlaps, we have developed precedence rules (Table 1) to resolve conflicts when a pixel is assigned different labels by separate postprocessing steps. For example, the region-filling algorithm that is applied to clear wood will create overlaps with knot regions. Because it is important to distinguish knots, we give those regions preference over clear wood regions. Whenever clear wood overlaps another defect type, clear wood surrenders its pixel label at that specific point. Because splits and decay can appear inside of knots, they are given precedence over knots whenever a conflict occurs. Included bark has not been addressed by the current system, so bark assumes the highest precedence.

An example of merging the result is shown in Fig. 7. Using the original image given in Fig. 1a, the background is detected and an ANN assigns tentative labels, as shown in Fig. 7b. Morphological postprocessing is conducted separately for each label type. The individual results are combined in Fig. 7c. Subjectively, postprocessing results in a considerable improvement for this example.

## DISCUSSION AND CONCLUSION

Artificial neural networks have been proven to give good results statistically for several defect types and for several species of hardwood. However, spurious pixel misclassifications often remain from ANN labeling, largely because our implementation heavily emphasizes local information. To correct for this, we have begun to develop a postprocessing methodology that is rule-based, applying refinement steps that are tailored to the individual types of defect. Because much of the refinement is related to region shape, the tools of mathematical morphology have been particularly effective in our experiments. Our current results with knots, bark, and split regions demonstrate impressive visual successes. These results need to be validated quantitatively, however, in future work.

## ACKNOWLEDGEMENTS

This work was supported in part by USDA NRI grant #98-35504-6581.

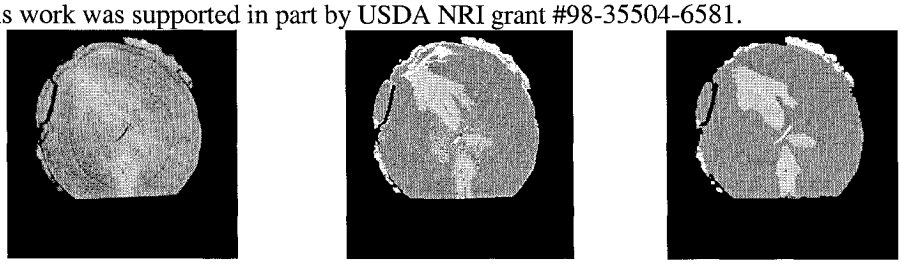

(a) (b) (c)

**Figure 7.** Example to illustrate the improvements that can result from postprocessing. (a) Original CT image, repeated from Figure 1a. (b) Initial labels assigned by ANN. (c) Combined result of postprocessing. The split near the center has been enlarged slightly (by morphological dilation) to make it easier to see.

## REFERENCES


1. Richards, D.B, Adkins, W.K., Hallock, H., and Bulgrin, E.H., "Simulation of hardwood log sawing", Forest Product Lab, Madison WI, Res. Pap. FPL-355, pp. 7 (1979).
2. Tsolakides, J.A, "A simulation model for log yield study", *Forest Products Journal*, **Vol. 19**, No. 7, pp. 21-26 (1969).
3. Wagner, F.G., Harless, T.E.G., Steele, P.H., Taylor, F.W., Yadama, V., and McMillin, C.W., "Production Management of Wood Products: Technology for the 90's", In *Proceedings of Process Control*, Athens GA, The University of Georgia, Athens GA, 1990, pp. 77-88.
4. Burgess, A.E. "Potential application of imaging techniques to wood products.", In *Proceedings of 1st International Conference on Scanning Technology in Sawmilling.* Miller-Freeman Publ., San Francisco, CA., 1985, pp. VII 1-13.
5. Taylor, F. W., Wagner, J. F. G., McMillin, C. W., Morgan, I. L., and Hopkins, F. F., "Locating knots by industrial tomography – a feasibility study.", *Forest Products Journal,* **Vol. 34**, No. 5, pp. 42-46 (1984).
6. Occeña, L. G., "Computer integrated manufacturing issues related to the hardwood log sawmill." *Journal of Forest Engineering,* **Vol. 3**, No. 1, pp. 39-45 (1991).
7. Zhu, D. P., Conners, R.W, Schmoldt, D.L., "Nondestructive evaluation of hardwood logs using automated interpretation of CT images", In *Proceedings, Review of Progress in Quantitative Nondestructive Evaluation*, edited by Thompson, D.O., and Chimenti D.E., Plenum Press, New York 1993, **Vol. 12**, pp. 2257-2264.
8. Bhandarkar, S.M., Faust, T., and Tang, M., "A System for Detection of Internal Log Defects by Computer Analysis of Axial CT Images," *Proceedings of IEEE International Workshop Applied Computer Vision*, Sarasota, FL, Dec. 2-4, 1996, pp. 258-263.
9. Li, P., Abbott, A. L., and Schmoldt, D. L., "Automated analysis of CT images for the inspection of hardwood logs", In *Proceedings of the 1996 IEEE International Conference on Neural Networks*, Washington, D.C., 1996, pp. 1744-1749.
10. Schmoldt, D. L., Li, P., and Abbott, A. L., "Machine vision using artificial neural networks and 3D pixel neighborhoods," *Computers and Electronics in Agriculture,* **Vol. 16**, No. 3, pp. 255-271 (1997).
11. Schmoldt, D.L., He, J., and Abbott, A.L., "Automated labeling of log features in CT imagery of multiple hardwood species." *Wood and Fiber Science*, **Vol. 32**, No. 3, pp. 287-300 (2000).
12. Sarigul, E., Abbott, A.L., and Schmoldt, D.L., "Rule-Driven Defect Detection in CT Images of Hardwood Logs", *4th International Conference on Image Processing and scanning of wood*, Kline, D.E., and Abbott, A.L. (Eds.), Mountain Lake, Virginia, 2000, pp. 37-49.
13. Matheron, G., *Random sets and integral geometry,* John Wiley, New York, 1975.
14. Serra, J., *Image analysis and mathematical morphology,* Academic Press, London, 1982
15. Haralick, R.M., Sternberg, S.R., and Zhuang, X., "Image analysis using mathematical morphology," *IEEE Trans. Pattern Analysis and Machine Intelligence,* **PAMI-9**, 532-550 (1987).
16. Lantuéjoul, C., "Skeletonization in quantitative metallography", in *Issues of Digital Image Processing*, edited by R.M. Haralick, and S.C. Simon, Sijthoff and Noordhoff, Groningen, The Netherlands, 1980, pp. 107-135.
17. Soille, P., *Morphological Image Analysis,* Springer-Verlag, Berlin, 1998.